Mineralogical Magazine, December 2014, Vol. 78(7), pp. 1613–1627

Innsbruckite, $Mn_{33}(Si_2O_5)_{14}(OH)_{38}$ – a new mineral from the Tyrol, Austria

HANNES KRÜGER[1,*], PETER TROPPER[1], UDO HAEFEKER[1], REINHARD KAINDL[2], MARTINA TRIBUS[1], VOLKER KAHLENBERG[1], CHRISTOPH WIKETE[3], MARTIN R. FUCHS[4] AND VINCENT OLIERIC[4]

[1] Institute of Mineralogy and Petrography, University of Innsbruck, Innrain 52, 6020 Innsbruck, Austria
[2] MATERIALS – Institute for Surface Technologies and Photonics, JOANNEUM RESEARCH Forschungsgesellschaft mbH, Leobner Strasse 94, 8712 Niklasdorf, Austria
[3] Material Technology Innsbruck (MTI), University of Innsbruck, Technikerstramße 13, 6020 Innsbruck, Austria
[4] Swiss Light Source, Paul Scherrer Institute, 5232 Villigen, Switzerland

[*Received 30 March 2014; Accepted 25 May 2014; Associate Editor: S. Krivovichev*]

ABSTRACT

A description of the new mineral innsbruckite, $Mn_{33}(Si_2O_5)_{14}(OH)_{38}$, a hydrous manganese phyllosilicate found in Tyrol, Austria is given. The crystal structure was determined by single-crystal synchrotron radiation diffraction experiments at the X06DA beamline at the Swiss Light Source (Paul Scherrer Institute, Villigen, Switzerland). The space group is *Cm* and lattice parameters are a = 17.2760(19), b = 35.957(5), c = 7.2560(8) Å, β = 91.359(7)º, V = 4506.1(10) Å^3, Z = 2. Innsbruckite belongs to the group of modulated 1:1 layer silicates and is chemically and structurally quite closely related to bementite, $Mn_7(Si_2O_5)_3(OH)_8$. The chemical analysis revealed a close to ideal composition with only minor amounts of Al, Fe and Mg. Using Liebau's nomenclature for silicate classification the silicate anion can be described as an unbranched *siebener* single layer. Innsbruckite shows a complex topology of the silicate sheet, exhibiting 4-, 5-, 6- and 8-membered rings. The silicate sheet is fully characterized using vertex symbols, and its topology is compared to those in other complex sheet silicates. Furthermore, the structural investigation is complemented with Raman spectroscopic studies.

KEYWORDS: innsbruckite, new mineral, phyllosilicate, Austria.

Introduction

THE new mineral innsbruckite has been found at a location 20 km southeast of Innsbruck, Austria. The mineral and name have been approved (2013-038, Krüger *et al*., 2013) by the International Mineralogical Association's Commission on New Minerals, Nomenclature and Classification. Innsbruckite belongs to the class of hydrous manganese phyllosilicate minerals (Liebau, 1985; Guggenheim and Eggleton, 1988), which generally exhibit complex types of silicate anions (for more recent examples see Yakovenchuk *et al.*, 2007, and references therein). Using the nomenclature of Liebau (1985), innsbruckite is a single layer silicate, with unbranched fundamental chains of periodicity seven. However, this classification cannot describe the complex topology which is generated by linkage of SiO_4 tetrahedra within the sheet. Graph theory (Delgado-Friedrichs and O'Keeffe, 2005; Blatov *et al.*, 2010) allows one to further characterize and compare the silicate anion based on topological features such as types of rings and nodes.

Mindat.org lists ~170 localities (Ralph, 2014) for the chemically closely related mineral bementite; all of them are potential locations to find innsbruckite, especially those with low iron content. Structural and Raman properties will allow one to distinguish easily between these minerals.

* E-mail: Hannes.Krueger@uibk.ac.at
DOI: 10.1180/minmag.2014.078.7.06

Occurrence and appearance

Innsbruckite (IMA 2013-038) was discovered at the interface between a serpentinite body and cherts at a locality near Staffelsee (Geier) in the innermost Navis valley, Tyrol, Austria (47º08′27″N, 11º37′31″E) at an elevation of ~2700 m AMSL (Fig. 1).

Geologically, these rocks belong to an Austroalpine Nappe called the Tarntal Mesozoic. The serpentinite belongs to the Reckner Complex and the cherts are part of the Ruhpolding Formation. The sample was collected by Klier (2005) while conducting field-work for a diploma thesis.

Associated minerals are rhodochrosite, friedelite, tephroite, spessartine, calcite, apatite and baryte. This mineral assemblage probably formed in deep-water Mn-rich sediments, upon which exhumed mantle rocks were juxtaposed. During the Eo-Alpine blueschist facies overprint (Dingeldey *et al.*, 1997), the assemblage tephroite + rhodochrosite + spessartine formed (Klier and Tropper, 2005; Klier *et al.*, 2007). Innsbruckite and friedelite crystallized over tephroite during a later hydration stage after the blueschist-facies metamorphic overprint, involving H_2O- and SiO_2-rich fluids along the model reaction 33 tephroite + 23 quartz + 38 H_2O = 2 innsbruckite; 33 Mn_2SiO_4 + 23 SiO_2 + 38 H_2O = 2 $Mn_{33}Si_{28}O_{70}(OH)_{38}$.

Innsbruckite occurs as thin platy crystals. The form of the plates is probably {001}. In thin section, the platelets appear as needle-like, elongated sections with sizes to ~150 μm (Fig. 2). The crystals are nearly colourless in transmitted light.

FIG. 1. Outcrop of the interface between serpentinite (below) and cherts. The length of the outcrop is ~2 m.

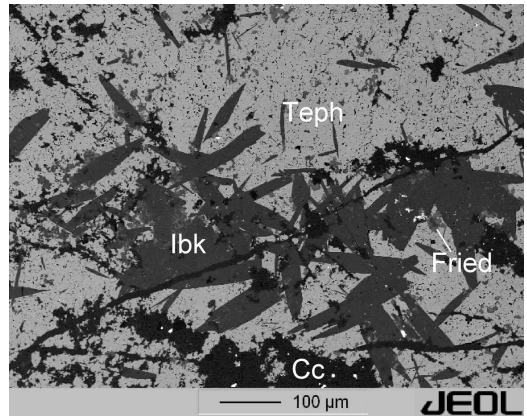

FIG. 2. Scanning electron microscope image (back-scattered electrons) of the assemblage tephroite (Teph) + innsbruckite (Ibk) + friedelite (Fried) + calcite (Cc).

Analytical methods

Electron microprobe analysis

The chemical composition was analysed using a Jeol JXA 8100 Superprobe (15 keV, 10 nA, spot size 1 μm). Standards used are listed in Table 1.

Diffraction experiments

A single crystal 45 μm × 15 μm × 15 μm was extracted mechanically from a thin section and glued to the tip of a thinned glass fibre. Crystallographic experiments were performed on the superbend magnet X06DA beamline at the Swiss Light Source (Paul Scherrer Institute, Villigen, Switzerland) equipped with a multi-axis PRIGo goniometer (Glettig *et al.*, 2011) and a Pilatus2M-F detector. Fine sliced images (1800 frames with 0.1º oscillation, integration time 0.5 s per frame) were collected with ω rotation and a focused beam size of 80 μm × 45 μm (h × v) at 17.5 keV, resulting in a total photon flux of 15×10^9 photons s^{-1}. The detector was set at 120 mm from the sample and was offset vertically by 67 mm to enhance the resolution of the data (0.70 Å resolution at the top edge of the detector). Data reduction was performed using *XDS* (Kabsch, 2010) and included Lorentz and polarization corrections.

The extinction symbol *C*1-1 was derived from the observed reflection condition of $h + k = 2n$. The structure was solved using *Sir2011* (Burla *et al.*, 2012) in space group *Cm*. Difference Fourier maps were used to complete the model and the

TABLE 1.Results of the electron microprobe analysis; averages of five spot analyses.

Constituent	wt.%	Range	e.s.d.	Probe standard
SiO_2	38.65	38.08–38.96	0.34	quartz
Al_2O_3	0.23	0.16–0.29	0.05	corundum
FeO	0.32	0.26–0.37	0.06	almandine
MnO	51.8	51.21–52.17	0.39	rhodonite
MgO	1.20	1.12–1.30	0.08	MgO
Cl	0.02	0.01–0.05	0.02	atacamite
H_2O	7.91	7.80–7.96	0.06	
F,Cl=O	0.0	0.0–0.01	0.00	
Total	100.12	98.94–100.78	0.69	

e.s.d. - estimated standard deviation.

refinement was performed with the program *Jana2006* (Petříček *et al.*, 2006). After all non-hydrogen atoms were found, inversion twinning and anisotropic displacement parameters were added to the refinement. In a last step, hydrogen atoms were located in difference Fourier maps and included in the structure model. Hydrogen atom locations were consistent with bond valence calculations. Isotropic displacement parameters of the hydrogen atoms were constrained to $1.2U_{eq}$ of their host oxygen atoms. Distances between O–H were restrained to 0.82(1) Å (Allen, 1986). The final twin fraction is 0.38(1). No additional symmetry was detected using the *ADDSYM* algorithm (Spek, 2009).

Data collection and refinement details are listed in Table 2. Atom coordinates and equivalent isotropic displacement parameters are listed in Table 3. Anisotropic displacement parameters can be found in the supplementary material, which has been deposited with the Principal Editor of *Mineralogical Magazine* and is available from www.minersoc.org/pages/e_journals/dep_mat_mm.html.

Optical microscopy

Investigation of optical properties was performed using a standard petrographic microscope and thin sections. Because of the small size of the innsbruckite crystals, the results are limited.

Raman spectroscopy

A Labram HR-800 confocal Raman-spectrometer (Horiba) was used to record the spectra. The system is equipped with an open-electrode charge-coupled device (CCD) with 1024 × 256 pixels (pixel size 43 μm) as detector and the 532 nm emission line of a 30 mW Nd:YAG laser was used for excitation. Raman spectra were recorded with a sample rotation of 90º through a 100 × objective with a numerical aperture of 0.9 using a grating with 1800 mm^{-1}. The confocal pinhole aperture was 1000 μm and the width of the entrance slit was 100 μm. The resolution of 1.4 cm^{-1} was determined by measuring the Rayleigh line. The system was calibrated using a neon lamp. Unpolarized spectra of randomly oriented polished grains were recorded in the range 100 to 1250 cm^{-1} and 3520 to 3700 cm^{-1} using the spectroscopic software suite *LabSpec 5* (Horiba Jobin Yvon S.A.S., 2010).

Nanoindentation

The hardness of three grains was determined using depth-sensing nanoindentation experiments utilizing a Nano Test Vantage apparatus (Micro Materials Ltd., Wrexham, UK). Indentation tests were performed with a Berkovich diamond indenter, using forces of 10 and 20 mN.

Results

Chemical composition

The chemical composition as averaged from five spot analyses is listed in Table 1. The empirical formula (based on 108 oxygen atoms per formula unit) is $Mn_{31.58}Fe_{0.19}Mg_{1.29}Si_{27.82}Al_{0.20}O_{108}H_{37.97}$, and the simplified formula on the basis of the structural model is $Mn_{33}(Si_2O_5)_{14}(OH)_{38}$. The oxide weight percentages corresponding to the simplified (idealized) formula are MnO: 53.62, SiO_2: 38.54 and H_2O: 7.84.

TABLE 2. Experimental details.

Crystal data	
Space group	*Cm*
a, *b*, *c* (Å)	17.2760(19), 35.957(5), 7.2560(8)
β (º)	91.359(7)
Volume (Å^3)	4506.1(10)
Formula	$Mn_{33}(Si_2O_5)_{14}(OH)_{38}$
Formula weight	4365.6
Z	2
D_{calc} (g cm^{-3})	3.216
Crystal size (μm)	45 × 15 × 15
Data collection	
Diffractometer	Beamline X06DA, Swiss Light Source Multi-axis goniometer PRIGo PILATUS2M-F detector
Wavelength (Å); Energy (keV)	0.7085; 17.5
Detector to sample distance (mm)	120
Oscillation range	0.1º
No. of frames measured	1800
Time of exposure (s)	0.5
Reflection ranges	$-19 \leqslant h \leqslant 18$; $-43 \leqslant k \leqslant 51$; $-6 \leqslant l \leqslant 10$
Reflections measured	13,293
R_{int}	0.0143
Refinement details	Full matrix least-squares on *F*
Unique reflections	8409
Observed unique refl. ($I>3\sigma(I)$)	7981
Final *R* values, $I > 3\sigma(I)$	$R = 0.0219$; $wR = 0.0281$
Final *R* values (all data)	$R = 0.0235$; $wR = 0.0284$
S (all data)	1.43
Refined parameters	843
Weighting scheme	$w = 1/(\sigma^2 (F)+0.0001F^2)$
Final $\Delta\rho_{min}$; $\Delta\rho_{max}$ (e Å^{-3})	–0.39; 0.37

Crystal structure

Innsbruckite is single layer silicate (monophyllosilicate), which exhibits a previously unknown topology of the tetrahedral silicate sheet. The tetrahedral sheets consist of 8-, 6-, 5- and 4-membered rings in the ratio 2:9:2:1, respectively (Fig. 3). The silicate sheets alternate with continuous layers of edge-sharing MnO_6 octahedra. The free apices of the silicate layer connect to both neighbouring octahedral layers (Fig. 4), and therefore one half of the tetrahedra point in one direction and the other half point in the opposite direction [directedness U and D of Liebau (1985)]. Hydrogen atoms (not shown in Figs 3 and 4) are bonded to the oxygen atoms not bridging between tetrahedra and octahedra, at the 'surface' of the octahedral layers.

Using the silicate nomenclature of Liebau (1985), monophyllosilicates show a dimensionality (***D***) of 2, and a multiplicity (***M***) of 1. In the structure of innsbruckite all silicate tetrahedra are connected to three neighbouring tetrahedra, and hence the connectedness (***s***) is 3. The silicate sheet can be subdivided into unbranched (***uB***) fundamental chains showing a periodicity (***P***) of 7 and are parallel to **a**. Two symmetry-independent fundamental chains are present in the structure, Si1–Si7 and Si8–Si14 (Fig. 3). Thus the structural formula after Liebau (1985) and Klein and Liebau (2008) takes the form $Mn_{33}\{\boldsymbol{uB},7,1^2_\infty\}[Si_{28}O_{70}](OH)_{38}$[†]. To the best of our knowledge no other minerals or synthetic structures with *siebener* single silicate layers are known.

[†] the parameters inside the curly brackets are $\{\boldsymbol{B},\boldsymbol{P},\boldsymbol{M}^{\boldsymbol{D}}_\infty\}$.

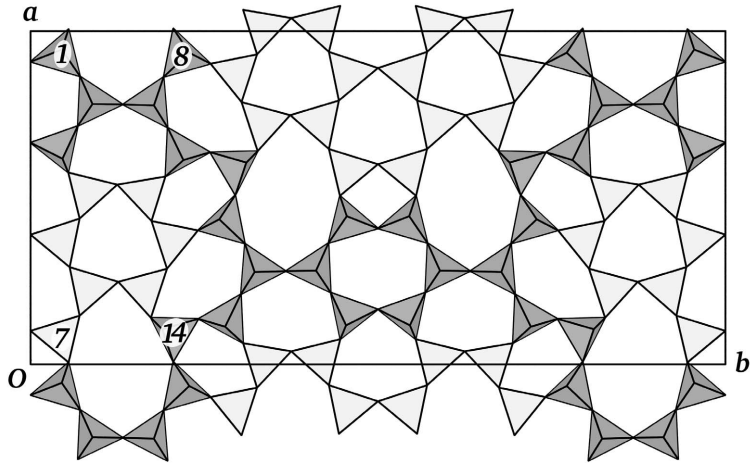

FIG. 3. The silicate sheet, exhibiting unbranched fundamental chains of periodicity 7 (Si1−Si7 and Si8−Si14, respectively). 'Islands' of three connected 6-membered rings (bright tetrahedra) exhibit reversed directedness of the tetrahedra. Program: *DRAWxtl* (Finger *et al.*, 2007).

Optical and physical properties

Microscopy investigation showed that innsbruckite is optically biaxially negative, with a small angle $2V_x$, as expected for sheet silicates. The optical sign of elongation is length positive (length slow). Direct measurement of 2V was not possible because no suitable grains were located in the thin sections. Extracted fragments were too small for spindle stage measurements. Furthermore, weak pleochroism was observed. An average refractive index of 1.678 was calculated from the Gladstone−Dale relationship (empirical formula) using the constants of Eggleton (1991). Because of the small size of the crystallites, physical properties such as streak, lustre, cleavage, parting, fracture and density could not be determined.

The nanoindentation experiments showed an averaged Berkovich hardness of 7.9(5) GPa, corresponding to a Vickers hardness of 740(50) HV. Consequently, the Mohs hardness is 6.

Because of chemical substitution (Mg and Al) the calculated density is smaller for the empirical formula (3.191 g cm^{-3}) compared to the value calculated for the idealized composition (Table 2).

Raman spectroscopy

The Raman spectrum of a randomly oriented grain with a 90º sample rotation between the data collections is given in Fig. 5. A list of observed Raman peaks is given in Table 4. Innsbruckite shows strong spectroscopic anisotropy as peak intensities between 100 and 1250 cm^{-1} vary extensively as a function of orientation. A group of three medium to strong peaks in the region 580−650 cm^{-1} are assumed to be characteristic for innsbruckite in addition to a sharp peak at

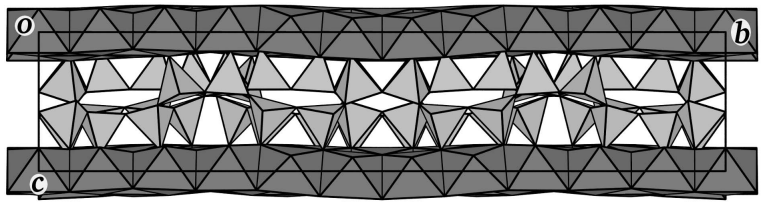

FIG. 4. The tetrahedral silicate sheet, sandwiched between two octahedral MnO_6 sheets. Program: *DRAWxtl* (Finger *et al.*, 2007).

TABLE 3. Atom parameters.

Atom	*x*/*a*	*y*/*b*	*z*/*c*	U_{eq}
Mn1	−0.00007(5)	0	−0.00641(11)	0.01108(18)
Mn2	−0.00075(3)	0.091165(12)	−0.00791(9)	0.01243(14)
Mn3	−0.00492(3)	0.182345(12)	−0.02038(8)	0.01218(14)
Mn4	−0.50420(3)	0.224898(12)	−0.01923(7)	0.01110(13)
Mn5	−0.00418(3)	0.365769(13)	0.02053(8)	0.01213(14)
Mn6	−0.00187(3)	0.455546(12)	0.04824(8)	0.01168(15)
Mn7	−0.33416(3)	0.454773(12)	0.05570(8)	0.01212(15)
Mn8	−0.33838(3)	0.362738(13)	0.04441(8)	0.01144(14)
Mn9	−0.33658(3)	0.271428(14)	−0.02443(8)	0.01102(13)
Mn10	−0.33637(3)	0.178856(13)	−0.05503(7)	0.01121(14)
Mn11	−0.33534(3)	0.089416(13)	−0.02874(8)	0.01151(14)
Mn12	−0.33399(4)	0	−0.02555(11)	0.0127(2)
Mn13	−0.16928(4)	0.5	0.07795(10)	0.0126(2)
Mn14	−0.16961(3)	0.409540(13)	0.06113(8)	0.01208(15)
Mn15	−0.17083(3)	0.319539(15)	0.02426(8)	0.01155(14)
Mn16	−0.17120(3)	0.227531(13)	−0.04551(7)	0.01096(13)
Mn17	−0.16715(3)	0.135049(13)	−0.05803(8)	0.01211(15)
Mn18	−0.16700(3)	0.044561(13)	−0.04094(9)	0.01264(15)
Si1	−0.42383(5)	0.45743(2)	−0.37002(12)	0.0077(2)
Si2	−0.27431(5)	0.41440(2)	−0.32811(13)	0.0075(2)
Si3	−0.12420(5)	0.45781(2)	−0.31947(13)	0.0078(2)
Si4	0.02616(5)	0.41603(2)	−0.36719(12)	0.0079(2)
Si5	0.14143(5)	0.45772(2)	−0.62259(12)	0.0081(2)
Si6	−0.21439(5)	0.09021(2)	0.33938(12)	0.0075(2)
Si7	−0.56869(5)	0.45749(2)	−0.63457(13)	0.0078(2)
Si8	−0.40252(5)	0.29837(2)	−0.61783(12)	0.0076(2)
Si9	−0.27746(5)	0.33094(2)	−0.36509(12)	0.0074(2)
Si10	−0.12553(5)	0.29017(2)	−0.39472(12)	0.0077(2)
Si11	−0.47742(5)	0.16785(2)	−0.39876(12)	0.0078(2)
Si12	−0.36990(5)	0.21682(2)	0.34882(12)	0.0078(2)
Si13	−0.21783(5)	0.17444(2)	0.32723(12)	0.0079(2)
Si14	−0.07279(5)	0.22185(2)	0.35587(12)	0.0076(2)
O1	0.05729(15)	0.04508(5)	−0.1566(4)	0.0103(7)
O2	0.1029(2)	0	0.1696(5)	0.0137(10)
O3	−0.27795(20)	0.5	−0.0898(5)	0.0124(9)
O4	−0.22433(16)	0.45386(6)	0.2054(4)	0.0135(7)
O5	−0.11769(14)	0.45679(5)	−0.0996(3)	0.0103(7)
O6	−0.0519(2)	0.5	0.2011(5)	0.0136(10)
O7	0.04732(19)	0.5	−0.1167(5)	0.0125(9)
O8	0.11718(15)	0.45404(6)	−0.8357(3)	0.0110(7)
O9	−0.28124(17)	0.04496(6)	−0.1663(4)	0.0126(7)
O10	−0.2203(2)	0	0.1172(5)	0.0129(10)
O11	−0.1067(2)	0	−0.1663(5)	0.0135(10)
O12	−0.55548(15)	0.45508(6)	−0.8508(4)	0.0105(7)
O13	0.05914(15)	0.13751(6)	−0.1359(4)	0.0122(7)
O14	0.10391(16)	0.09186(6)	0.1657(4)	0.0134(7)
O15	−0.27920(14)	0.41166(6)	−0.1091(3)	0.0101(7)
O16	−0.22710(16)	0.36196(7)	0.1797(3)	0.0141(7)
O17	−0.11890(15)	0.36717(6)	−0.1119(3)	0.0129(7)
O18	−0.05418(16)	0.40905(6)	0.1805(3)	0.0140(7)
O19	−0.45462(14)	0.08578(6)	−0.1521(3)	0.0105(7)
O20	−0.38643(15)	0.13469(6)	0.1195(3)	0.0123(7)
O21	−0.28260(16)	0.13327(6)	−0.1872(3)	0.0135(7)
O22	−0.21879(15)	0.08914(6)	0.1207(3)	0.0112(7)
O23	−0.10806(15)	0.08930(6)	−0.1715(3)	0.0122(7)
O24	−0.06020(15)	0.13716(6)	0.1227(4)	0.0134(7)
O25	−0.44999(14)	0.27043(6)	−0.1501(3)	0.0117(7)
O26	−0.39457(13)	0.31054(6)	0.1712(3)	0.0105(6)

Table 9 (*contd*.).

Atom	*x*/*a*	*y*/*b*	*z*/*c*	U_{eq}
O27	−0.28390(13)	0.32271(6)	−0.1491(3)	0.0095(6)
O28	−0.22644(14)	0.27007(7)	0.1216(3)	0.0126(7)
O29	−0.61896(14)	0.22299(6)	−0.1846(3)	0.0112(6)
O30	−0.55569(14)	0.18302(7)	0.1369(3)	0.0129(7)
O31	−0.45322(13)	0.17687(6)	−0.1898(3)	0.0103(6)
O32	−0.38695(13)	0.21999(6)	0.1309(3)	0.0099(6)
O33	−0.28398(15)	0.22726(6)	−0.1785(3)	0.0123(7)
O34	−0.22286(14)	0.17754(6)	0.1086(3)	0.0113(7)
O35	−0.11277(15)	0.18312(6)	−0.1796(3)	0.0124(7)
O36	−0.06488(13)	0.22836(6)	0.1390(3)	0.0101(6)
O37	−0.49440(13)	0.44523(6)	−0.5074(3)	0.0139(6)
O38	−0.35407(12)	0.42939(6)	−0.4248(3)	0.0110(6)
O39	−0.20847(12)	0.44370(6)	−0.3952(3)	0.0110(6)
O40	−0.06254(12)	0.42934(6)	−0.4107(3)	0.0119(6)
O41	0.07559(13)	0.44574(6)	−0.4801(3)	0.0149(6)
O42	−0.28470(12)	0.06805(6)	0.4329(3)	0.0137(6)
O43	−0.13618(12)	0.07128(6)	0.4264(3)	0.0121(6)
O44	−0.25247(12)	0.37369(5)	−0.4112(3)	0.0106(6)
O45	−0.46102(12)	0.12483(5)	−0.4581(3)	0.0106(6)
O46	−0.22031(13)	0.13275(5)	0.4126(3)	0.0119(6)
O47	0.00772(12)	0.20532(6)	0.4445(3)	0.0141(6)
O48	−0.36028(11)	0.32681(5)	−0.4740(3)	0.0105(6)
O49	−0.21318(12)	0.30361(6)	−0.4543(3)	0.0109(6)
O50	−0.56998(12)	0.17408(6)	−0.4340(3)	0.0115(6)
O51	−0.43645(13)	0.19411(6)	0.4524(3)	0.0150(6)
O52	−0.28956(12)	0.19726(6)	0.4137(3)	0.0133(6)
O53	−0.13776(12)	0.19154(6)	0.4095(3)	0.0135(6)
O54	−0.36350(12)	0.25836(5)	0.4321(3)	0.0124(6)
O55	−0.09811(12)	0.25905(6)	−0.5391(3)	0.0157(6)
O56	−0.39973(17)	0.5	−0.4260(4)	0.0118(8)
O57	−0.11105(16)	0.5	−0.3993(4)	0.0105(8)
O58	0.16517(16)	0.5	−0.5677(4)	0.0111(8)
O59	−0.59232(17)	0.5	−0.5730(4)	0.0112(8)
H2	0.101(3)	0	0.2831(15)	0.016457
H3	−0.273(3)	0.5	−0.2024(17)	0.014894
H4	−0.220(2)	0.4510(9)	0.3174(15)	0.016158
H6	−0.044(3)	0.5	0.3134(18)	0.016291
H7	0.033(3)	0.5	−0.225(2)	0.014977
H9	−0.286(2)	0.0491(9)	−0.2771(17)	0.015153
H10	−0.207(3)	0	0.227(2)	0.01543
H11	−0.106(3)	0	−0.2800(15)	0.016205
H13	0.0740(19)	0.1410(10)	−0.240(2)	0.014652
H14	0.110(2)	0.0877(10)	0.2761(17)	0.016044
H16	−0.230(2)	0.3643(10)	0.2922(15)	0.016926
H17	−0.124(2)	0.3651(10)	−0.2249(15)	0.015509
H18	−0.061(2)	0.4090(10)	0.2924(16)	0.01684
H20	−0.3597(18)	0.1298(9)	0.211(3)	0.014776
H21	−0.287(2)	0.1326(10)	−0.3006(15)	0.016232
H23	−0.112(2)	0.0958(9)	−0.2798(19)	0.014648
H24	−0.064(2)	0.1332(10)	0.2348(17)	0.016134
H25	−0.4608(19)	0.2703(10)	−0.2597(17)	0.014074
H28	−0.218(2)	0.2693(10)	0.2329(16)	0.015111
H30	−0.550(2)	0.1869(10)	0.2471(17)	0.015436
H33	−0.283(2)	0.2310(10)	−0.2910(16)	0.014805
H35	−0.107(2)	0.1863(10)	−0.2908(17)	0.014916

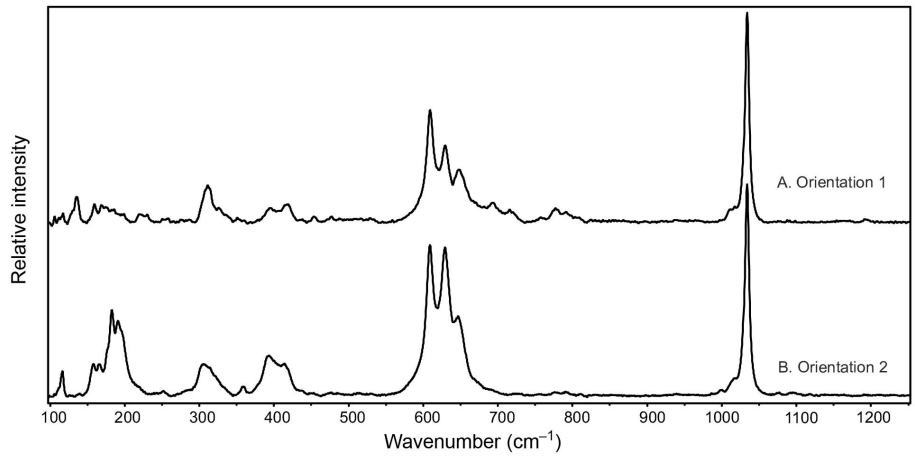

FIG. 5. The Raman spectrum of innsbruckite (100–1250 cm^{-1}) with 90º sample rotation between the data collections.

1032 cm^{-1}, which is the most intense peak in both orientations. In a Raman study of the complex double layer silicate stilpnomelane, a broad Si–O$_b$–Si (bridging oxygen) peak centred between 590 and 600 cm^{-1} with a shoulder near 505 cm^{-1} was described (Kuebler *et al.*, 2011). The breadth of the peak was attributed to the large size of the unit cell and modulated structure. Peaks above 900 cm^{-1} and below 400 cm^{-1} were assigned to Si–O$_{nb}$ (non-bridging oxygen) and lattice vibrations. In the range 550–730 cm^{-1} a minimum of seven partly overlapping peaks can be deconvoluted, and are presumably related to vibrations within the tetrahedra and translations of Mn (McKeown *et al.*, 1999*a*,*b*).

In Raman spectra of phyllosilicates, the number of OH peaks, their positions and relative intensities are controlled by the different structural environments of the OH groups (e.g. Johnston *et al.*, 1998). Figure 6 shows the wavenumber region between 3520 and 3700 cm^{-1}, which is dominated by several sharp and intense Raman peaks

TABLE 4. Raman spectrum of Innsbruckite.

cm^{-1}	Rel. intensity	cm^{-1}	Rel. intensity	cm^{-1}	Rel. intensity
108	vw	277	vw	609	m-s
114	vw	288	vw	629	m-s
118	vw-w	305	shoulder	649	m
131	shoulder	312	vw-w	671	vw
137	w	315	w	693	vw-w
160	w	322	vw	717	vw-w
169	w	327	vw-w	777	vw-w
178	shoulder	336	vw-shoulder	792	vw
185	w-m	352	vw	998	vw
193	w-m	360	vw-w	1010	vw
199	shoulder	394	w	1016	vw
221	vw	405	w	1032	s
231	vw	417	w	1190	vw
252	vw	455	vw-w		
259	vw	477	vw		

Key - vw: very weak; w: weak; m: medium; s: strong.

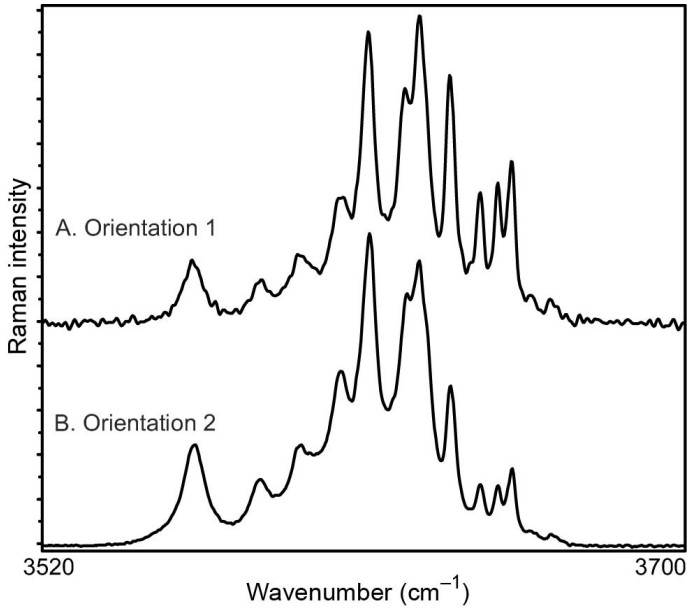

FIG. 6. The Raman spectrum of innsbruckite in the high frequency region.

representing the stretching modes of OH groups. The number of peaks suggests at least 6–8 dominating different structural environments for OH groups, in agreement with the crystal structure determination.

Discussion

Within the group of modulated 1:1 layer silicates (Guggenheim and Eggleton, 1988) or 'cation-rich' hydrous phyllosilicates with tetrahedron inversion (Liebau, 1985), innsbruckite is an example with continuous octahedral and continuous tetrahedral sheets. In such structures, tetrahedra of directedness U (up) and D (down) are present within one tetrahedral layer. Apical oxygen atoms of the tetrahedra point in opposite directions related to the basal plane of the silicate sheet. Also, these apical oxygen atoms link the silicate anion to both adjacent octahedral layers to form an alternating stacking of octahedral and tetrahedral sheets. Whether a 'modulation' (tetrahedron inversion) occurs is determined by the misfit of the mesh sizes of the octahedral (b_{oct}) and the tetrahedral (b_{tetr}) sheet. Structures without misfit show flat kaolinite-like layers and no tetrahedral inversion.

For increasing difference $b_{oct} - b_{tetr}$ several mechanisms for stress reduction are described by Liebau (1985) and Guggenheim and Eggleton (1988). The difference $b_{oct} - b_{tetr}$ gets larger with increasing size of the octahedral M cations and smaller with increasing size of the T cations. Following table 10.15 in Liebau (1985), with increasing difference, flat kaolinite-like layers become rolled or coiled structures (chrysotile for example). With larger differences, tetrahedral inversion occurs in antigorites. For a detailed discussion on the effects of misfit in serpentine minerals see for example Chernosky (1975), Deer *et al.* (2009) and references therein. For even larger misfits re-arrangement of the tetrahedral sheet changes its topology and creates the structures of pyrosmalite, bementite, and the apophyllite-group members.

In structures with tetrahedral inversion, regions of equal directedness (RED) can be identified in the $[T_2O_5]$ sheet. REDs may be stripes or islands of tetrahedra with the same directedness. For example, in antigorite the REDs are *vierer* multiple chains (Liebau, 1985; Deer *et al.*, 2009 and references therein), resulting in one-dimensional wavy deformation of the layers. In minerals of the pyrosmalite group, 6-membered rings have the same directedness, with each RED surrounded by three opposite REDs. Greenalite and caryopilite show REDs in the form of 'islands' of three 6-membered rings, which are connected by 5-, 6-, 7-

and 8-membered rings to form sheets with structural disorder (Guggenheim and Eggleton, 1998). Another single layer silicate with continuous tetrahedral and continuous octahedral sheets is bementite. In bementite REDs are one-dimensional and can be described as loop-branched *sechser* chains. Apophyllite exhibits 4-membered rings as RED.

A comparison between the ideal formulae of bementite (Heinrich *et al.*, 1994) and innsbruckite reveals similar compositions: for $Mn_7(Si_2O_5)_3(OH)_8$, oxide weight percentages of 53.44 MnO, 38.80 SiO_2 and 7.76 H_2O result. These values cannot be distinguished easily from the values for the ideal innsbruckite composition (see above). However, chemical analyses of bementite (Kato, 1963; Heinrich *et al.*, 1994; Dunn, 1995) show significant substitution of the octahedral cations by Fe, Zn and Mg. These substitutions cause a reduction of the octahedral layer compared to a pure Mn formulation, thus reducing misfit. Additionally, substitution of Al into tetrahedral sites will further decrease the octahedral-tetrahedral layer misfit. In the series of structures with increasing $b_{oct} - b_{tetr}$ difference (Liebau, 1985), innsbruckite is positioned next to bementite at a slightly higher $b_{oct} - b_{tetr}$, as the difference in bementite is reduced by the substitution as discussed above.

The geometry of the octahedra in bementite is generally more distorted than in innsbruckite. Distortion parameters after Robinson *et al.* (1971) are as quadratic elongation (*QE*) 1.172 and angle variance (*AV*) 494 for bementite, compared to much less distortion (QE_{max} 1.032 and AV_{max} 97) in innsbruckite.

As it is difficult to distinguish between bementite and innsbruckite based solely on chemical analysis, Raman spectroscopy or diffraction techniques are required to differentiate between the two minerals. Figure 7 compares the powder X-ray diffraction patterns of bementite and innsbruckite. A calculated powder pattern in tabular form is included in the supplementary material (deposited at www.minersoc.org/pages/e_journals/dep_mat_mm.html).

Two Mn-rich monophyllosilicates show structures without obvious misfit or tetrahedron inversion. One is guidottiite $Mn_2Fe(FeSiO_5)(OH)_4$ (Wahle *et al.*, 2010), where there is significant substitution of iron at octahedral and tetrahedral sites, thus reducing the lateral dimensions of the octahedral sheet and expanding the tetrahedral sheet. The resulting structure exhibits planar kaolinite-like layers with cronstedtite-$2H_1$ and $2H_2$ polytypes. Kellyite $Mn_2Al(AlSiO_5)(OH)_4$ (Peacor *et al.*, 1974) shows the same type of sheet. In this case, substitution of Al at octahedral and tetrahedral sites reduces the misfit.

The classification based on Liebau (1985) is a general tool for all silicate structures. However, it provides little information on the topology of a silicate sheet. As seen in Table 5, silicate sheets with different topologies may exhibit the same Liebau symbol. Consequently, for a detailed discussion and comparison of topological

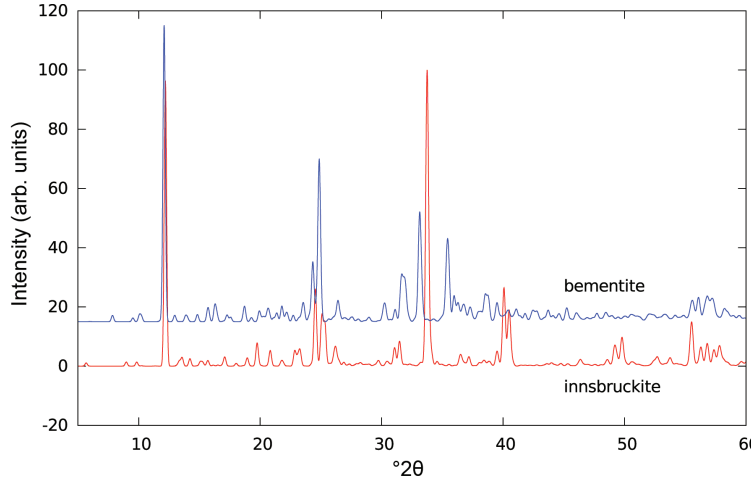

FIG. 7. Comparison of the powder patterns of bementite (Heinrich *et al.*, 1994) and innsbruckite. Both patterns are calculated for Cu$K\alpha_1$ using *Xpow* (Downs *et al.*, 1993).

TABLE 5. Examples of Q^3 connected silicate sheets with complex topologies (more than three types of rings).

Name/Composition	Liebau	RS	*ndv*	Fig.	Reference
Single-layer silicates					
$A_3REESi_6O_{15}{\cdot}xH_2O$	$\{\boldsymbol{uB},3,1^2_\infty\}$	$4^15^26^18^2$	4	9*a*	Karpov *et al.* (1977); Haile *et al.* (1997); Wang *et al.* (2007); Cadoni *et al.* (2010)
Dalyite	$\{\boldsymbol{uB},3,1^2_\infty\}$	$4^16^18^1$	2	9*h*	Fleet (1965)
Intersilite	$\{\boldsymbol{uB},5,1^2_\infty\}$	$5^26^28^1$	4	9*f*	Yamnova *et al.* (1996)
Varennesite	$\{\boldsymbol{hB},6,1^2_\infty\}$	$4^26^210^1$	2	9*e*	Grice and Gault (1995)
Pyrosmalite	$\{\boldsymbol{uB},6,1^2_\infty\}$	$4^36^212^1$	1	9*d*	Kato and Takeuchi (1983)
Bementite	$\{\boldsymbol{uB},6,1^2_\infty\}$	$5^16^17^1$	3	9*c*	Heinrich *et al.* (1994)
Innsbruckite	$\{\boldsymbol{uB},7,1^2_\infty\}$	$4^15^26^98^2$	5	9*b*	This work
VSH-11RbNa	$\{\boldsymbol{lB},8,1^2_\infty\}$	$4^66^28^312^1$	2	9*g*	Wang *et al.* (2002)
Double-layer silicates					
Tamaite	$\{\boldsymbol{hB},6,2^2_\infty\}$	$5^16^37^1$	3		Hughes *et al.* (2003)
Armbrusterite	$\{\boldsymbol{uB},6,2^2_\infty\}$	$5^46^27^28^1$	5		Yakovenchuk *et al.* (2007)
Bannisterite	$\{\boldsymbol{oB},7,2^2_\infty\}$	$5^26^47^2$	4		Heaney *et al.* (1992)
Stilpnomelane	$\{\boldsymbol{uB},9,2^2_\infty\}$	$5^26^38^1$	3		Guggenheim and Eggleton (1994)
Parsettensite	$\{\boldsymbol{lB},10,2^2_\infty\}$	$4^35^66^712^2$	4		Eggleton and Guggenheim (1994)

RS: ring symbol, *ndv*: number of distinct vertices.

aspects, further tools have to be employed. Using graph theory (Delgado-Friedrichs and O'Keeffe, 2005; Blatov *et al.*, 2010) to describe the topology of 2-dimensional nets formed by silicon atoms as vertices (nodes), innsbruckite exhibits a 2-periodic and 3-connected net. A ring symbol (Yakovenchuk *et al.*, 2007) or signature (Blatov *et al.*, 2010), which gives the type and relative frequency (superscript) of the rings is $4^15^26^98^2$. A more detailed description of the topology uses all present vertex symbols (VS) and their relative numbers (subscript): $(4{\cdot}6{\cdot}8)_2(5{\cdot}6^2)_3(5{\cdot}6{\cdot}8)_2(6^3)_3(6^2{\cdot}8)_4$. The VS for each vertex (Si atom) is given in Table 6. Innsbruckite shows four different types of rings (by the number of vertices) and five different types of nodes (by the VS symbol) within the 3-connected net. The highest symmetry which can be adopted by this net corresponds to plane group *c*2*mm*, and the transitivity is determined as 8(13)7, which indicates 8 kinds of vertices (different by coordination sequence), 13 kinds of edges, and 7 kinds of faces (different by symmetry). The D size or complexity of the net is 42. Figure 8 shows an embedding (realization) of the net using plane group *c*2*mm*. Faces (rings) of the same colour/shade are symmetrically equivalent. The embedding was derived using *Systre* (Delgado-Friedrichs and O'Keeffe, 2003) and plotted with *Gavrog* (Delgado-Friedrichs, 2013). A *Systre* archive file and a Table with the coordination sequences is included in the supplementary material (deposited at www.minersoc.org/pages/e_journals/dep_mat_mm.html).

TABLE 6. Vertex symbols for all vertices of the 2-periodic innsbruckite silicate net. Vertex numbers correspond to the number of the silicon atoms in provided structural data (Si*n*).

Vertex	Vertex symbol (VS)
1, 7	$4{\cdot}6{\cdot}8$
2, 6, 9, 13	$6^2{\cdot}8$
3–5	6^3
8, 14	$5{\cdot}6{\cdot}8$
10–12	$5{\cdot}6^2$

A comparison with the closely related bementite reveals the differences in the topology of the silicate sheet. The tetrahedral layer in bementite (Fig. 9*c*) is less complex, with three different types of rings (5-, 6- and 7-membered rings). As discussed above, the RED in bementite has one-dimensional character, whereas innsbruckite exhibits 'islands' of three 6-membered rings as REDs (bright nodes in Fig. 9*b*) and thus inducing

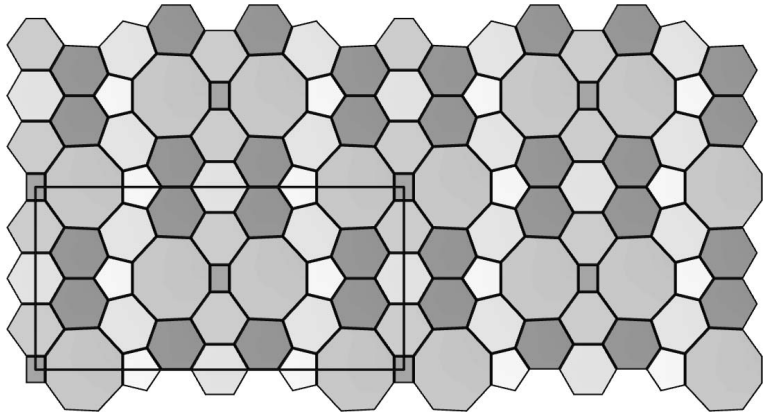

FIG. 8. The silicate layer of innsbruckite abstracted as a tiling of the plane (*c*2*mm*), the true symmetry in innsbruckite is lower (*cm*; Fig. 3). Colours symbolize different kinds of faces (rings). Image created using *3dt* (Delgado-Friedrichs, 2013).

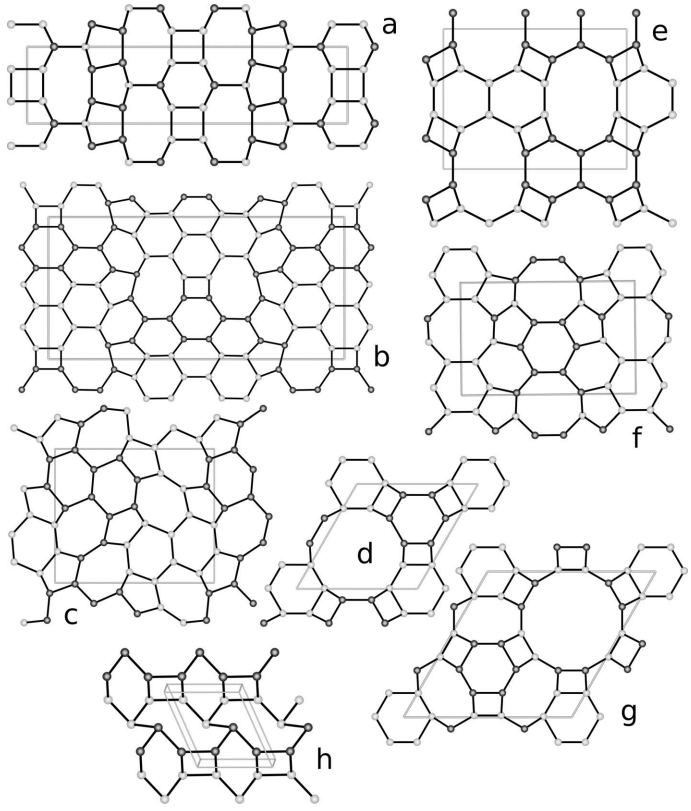

FIG. 9. Topology of related complex single layer silicates: (*a*) $A_3REESi_6O_{15}{\cdot}xH_2O$, (*b*) innsbruckite, (*c*) bementite, (*d*) pyrosmalite (structure of VSH-6CsK (Wang *et al.*, 2002) is shown), (*e*) varennesite, (*f*) intersilite, (*g*) VSH-11, and (*h*) dalyite. Spheres correspond to the centres of tetrahedra, with the free apex pointing either up (bright) or down (dark). For details and references see text and Table 5.

a two-dimensional undulation of the layers. No identical nodes exist between bementite and innsbruckite.

Table 5 shows a number of phyllosilicates with complex topology of the tetrahedral layer. In particular, silicate sheets with large periodicities and at least three different types of rings are listed. Looking at the topology of the Q^3 silicate sheet only, close similarities to the silicate layers in synthetic compounds described by Karpov *et al.* (1977), Haile *et al.* (1997), Wang *et al.* (2007) and Cadoni *et al.* (2010) can be recognized (compare Fig. 9*a*). The same types of rings occur and the maximal symmetry (*c*2*mm*) of the sheet is the same. The innsbruckite layer topology is generated by adding 6-membered rings to the ($4^1 5^2 6^6 8^2$)-sheet. However, both topologies share only one common node (4·6·8). Although lacking 4-membered rings, the sheet topology of intersilite (Fig. 9*f*) is related by sharing three nodes ($5{\cdot}6^2$, 5·6·8 and $6^2{\cdot}8$) with innsbruckite. The sheets in varennesite and pyrosmalite (see Table 5 and Fig. 9) exhibit larger rings. The synthetic compound of VSH-11RbNa showing a sheet topology with four ring types ($4^6 6^2 8^3 12^1$) was synthesized by Wang *et al.* (2002).

Considering the two-dimensional sheet topology only, a comparison with double layer silicates indicates that three of the five nodes of innsbruckite also occur in stilpnomelane. Tamaite, dalyite, and bannisterite have one, and parsettensite has two common nodes with innsbruckite. Some overview of double layer silicates can be found in Yakovenchuk *et al.* (2007).

Another complex silicate sheet is found in yakovenchukite (Krivovichev *et al.*, 2007). With 4-, 6- and 14-membered rings, its topology is not related. Complex sheets with Q^4 tetrahedra are found in nordite, bussyite, semenovite, and vladykinite. All of them show 4-, 5- and 8-membered rings. An overview is given in Chakhmouradian *et al.* (2014). An even more complex topology has been found in samfowlerite (Rouse *et al.*, 1994), a beryllium phyllosilicate with Q^3 and Q^4 units within the layer. For an overview of complex beryllosilicate layers with Q^3 and Q^4 tetrahedra and their topologies see Huminicki and Hawthorne (2002).

The directedness of the tetrahedra inside a silicate sheet may lead to different geometrical isomers (Moore, 1975) of the same topology. Nomenclature for geometrical isomers is described by Krivovichev (2005).

Type material

Holotype material is deposited in the collections of the Museum of Natural History in Vienna (Naturhistorisches Museum Wien), Burgring 7, 1010 Vienna, Austria (registration number N 9580).

Acknowledgements

The authors are grateful to Reinhard Klier for providing the sample material, to Uwe Kolitsch for reviewing the new mineral proposal, and to Hans-Joachim Klein for help with *CRYSTANA*.

References

Allen, F.H. (1986) A systematic pairwise comparison of geometric parameters obtained by X-ray and neutron diffraction. *Acta Crystallographica*, **B42**, 515–522.

Blatov, V.A., O'Keeffe, M. and Proserpio, D.M. (2010) Vertex-, face-, point, Schläfli-, and Delaney-symbols in nets, polyhedra and tilings: recommended terminology. *CrystEngComm*, **12**, 44–48.

Burla, M.C., Caliandro, R., Camalli, M., Carrozzini, B., Cascarano, G.L., Giacovazzo, C., Mallamo, M., Mazzone, A., Polidori, G. and Spagna, R. (2012) *SIR2011*: a new package for crystal structure determination and refinement. *Journal of Applied Crystallography*, **45**, 357–361.

Cadoni, M., Cheah, Y.L. and Ferraris, G. (2010) New RE microporous heteropolyhedral silicates containing $4^1 5^1 6^1 8^2$ tetrahedral sheets. *Acta Crystallographica*, **B66**, 158–164.

Chakhmouradian, A.R., Cooper, M.A., Ball, N., Reguir, E.P., Medici, L., Abdu, Y.A. and Antonov, A.A. (2014) Vladykinite, $Na_3Sr_4(Fe^{2+}Fe^{3+})Si_8O_{24}$: A new complex sheet silicate from peralkaline rocks of the Murun complex, eastern Siberia, Russia. *American Mineralogist*, **99**, 235–241.

Chernosky, J.V., Jr. (1975) Aggregate refractive indices and unit cell parameters of synthetic serpentine in the system $MgO–Al_2O_3–SiO_2–H_2O$. *American Mineralogist*, **60**, 200–2008.

Deer, W.A., Howie, R.A. and Zussman, J. (editors) (2009) *Rock-Forming Minerals. Volume 3B: Layered Silicates Excluding Micas and Clay Minerals*. Geological Society Publishing House, 2nd edition, 320 pp.

Delgado-Friedrichs, O. (2013) *The Gavrog Project: systre 1.2.0 and 3dt 0.6.0*. http://gavrog.org. Accessed May 2014.

Delgado-Friedrichs, O. and O'Keeffe, M. (2003) Identification of and symmetry computation for crystal nets. *Acta Crystallographica*, **A59**, 351–360.

Delgado-Friedrichs, O. and O'Keeffe, M. (2005) Crystal

nets as graphs: terminology and definitions. *Journal of Solid State Chemistry*, **178**, 2480–2485.

Dingeldey, C., Dallmeyer, D., Koller, F. and Massonne, H.J. (1997) P-T-t history of the Lower Austroalpine Nappe Complex in the 'Tarntaler Berge' NW of the Tauern Window: implications for the geotectonic evolution of the central Eastern Alps. *Contributions to Mineralogy and Petrology*, **129**, 1–19.

Downs, R.T., Bartelmehs, K.L., Gibbs, G.V. and Boisen, M.B., Jr. (1993) Interactive software for calculating and displaying X-ray or neutron powder diffractometer patterns of crystalline materials. *American Mineralogist*, **78**, 1104–1107.

Dunn, P.J. (1995) *Franklin and Sterling Hill, New Jersey: The World's Most Magnificent Mineral Deposits*. The Franklin-Ogdensburg Mineralogical Society, Franklin, New Jersey, USA.

Eggleton, R.A. (1991) Gladstone-Dale constants for the major elements in silicates; coordination number, polarizability, and the Lorentz-Lorentz relation. *The Canadian Mineralogist*, **29**, 525–532.

Eggleton, R.A. and Guggenheim, S. (1994) The use of electron optical methods to determine the crystal structure of a modulated phyllosilicate: Parsettensite. *American Mineralogist*, **79**, 426–437.

Finger, L.W., Kroeker, M. and Toby, B.H. (2007) *DRAWxtl*, an open-source computer program to produce crystal structure drawings. *Journal of Applied Crystallography*, **40**, 188–192.

Fleet, S.G. (1965) The crystal structure of dalyite. *Zeitschrift für Kristallographie*, **121**, 349–368.

Glettig, W., Vitins, M., Schwarb, A., Maag, S. and Schulze-Briese, C. (2011) First results from PRIGO III, the parallel robotics inspired goniometer for protein crystallography. *Proceedings of the Euspen 11th International Conference*, **2**, 31.

Grice, J.D. and Gault, R.A. (1995) Varennesite, a new species of hydrated Na-Mn silicate with a unique monophyllosilicate structure. *The Canadian Mineralogist*, **33**, 1073–1081.

Guggenheim, S. and Eggleton, R.A. (1988) Crystal chemistry, classification, and identification of modulated layer silicates. Pp. 675–725 in: *Hydrous Phyllosilicates (Exclusive of Micas)* (S.W. Bailey, editor). Reviews in Mineralogy, **19**. Mineralogical Society of America, Washington DC.

Guggenheim, S. and Eggleton, R.A. (1994) A comparison of the structures and geometric stabilities of stilpnomelane and parsettensite: a distance least-squares (DLS) study. *American Mineralogist*, **79**, 438–442.

Guggenheim, S. and Eggleton, R.A. (1998) Modulated crystal structures of greenalite and caryopilite; a system with long-range, in-plane structural disorder in the tetrahedra sheet. *The Canadian Mineralogist*, **36**, 163–179.

Haile, S.M., Wuensch, B.J., Laudise, R.A. and Maier, J. (1997) Structure of $Na_3NdSi_6O_{15}{\cdot}2H_2O$ – a layered silicate with paths for possible fast-ion conduction. *Acta Crystallographica*, **B53**, 7–17.

Heaney, P.J., Post, J.E. and Evans, H.T. (1992) The crystal structure of bannisterite. *Clays and Clay Minerals*, **40**, 129–144.

Heinrich, A.R., Eggleton, R.A. and Guggenheim, S. (1994) Structure and polytypism of bementite, a modulated layer silicate. *American Mineralogist*, **79**, 91–106.

Horiba Jobin Yvon S.A.S. (2010) *LabSpec 5*. Longjumeau Cedex, France.

Hughes, J.M., Rakovan, J., Bracco, R. and Gunter, M.E. (2003) The atomic arrangement of the ganophyllite-group modulated layer silicates as determined from the orthorhombic dimorph of tamaite, with the elusive 16.8 Å ganophyllite-group superstructure revealed. *American Mineralogist*, **88**, 1324–1330.

Huminicki, D.M. and Hawthorne, F.C. (2002) Refinement of the crystal structure of aminoffite. *The Canadian Mineralogist*, **40**, 915–922.

Johnston, C.T., Helsen, J., Schoonheydt, R.A., Bish, D.L. and Agnew, S.F. (1998) Single-crystal Raman spectroscopic study of dickite. *American Mineralogist*, **83**, 75–84.

Kabsch, W. (2010) *XDS. Acta Crystallographica*, **D66**, 125–132 .

Karpov, O.G., Pushcharovskii, D.Y., Pobedimskaya, E.A., Burshtein, I.F. and Belov, A.N.V. (1977) The crystal structure of the rare-earth silicate $NaNdSi_6O_{13}(OH)_2{\cdot}nH_2O$. *Soviet Physics Doklady*, **22**, 464–466.

Kato, T. (1963) New data on the so-called bementite. *Journal of the Mineralogical Society of Japan*, **6**, 93–103.

Kato, T. and Takeuchi, Y. (1983) The pyrosmalite group minerals; I, structure refinement of manganpyrosmalite. *The Canadian Mineralogist*, **21**, 1–6.

Klein, H.J. and Liebau, F. (2008) Computerized crystal-chemical classification of silicates and related materials with *CRYSTANA* and formula notation for classified structures. *Journal of Solid State Chemistry*, **181**, 2412–2417.

Klier, R. (2005) *Das Tarntal Mesozoikum: Petrologie und Geologie einer enigmatischen Einheit in den Ostalpen*. Diploma thesis, University of Innsbruck, Austria.

Klier, R. and Tropper, P. (2005) Amphibole zonation as a function of P-T-XCO_2-fO_2 in blueschists from the Austroalpine Reckner Nappe (Eastern Alps, Austria). *Mitteilungen der Österreichischen Mineralogischen Gesellschaft*, **150**, 69.

Klier, R., Tropper, P. and Rockenschaub, M. (2007) The metamorphic evolution of blueschists of the Tarntal Nappe. *Mitteilungen der Österreichischen*

Mineralogischen Gesellschaft, **153**, 64.

Krivovichev, S. (2005) Topology of microporous structures Pp. 17–68 in: *Micro- and Mesoporous Mineral Phases* (G. Ferraris and S. Merlino, editors). Reviews in Mineralogy and Geochemistry, **57**. Mineralogical Society of America and the Geochemical Society, Chantilly, Virginia, USA.

Krivovichev, S.V., Pakhomovsky, Y.A., Ivanyuk, G.Y., Mikhailova, J.A., Men'shikov, Y.P., Armbruster, T., Selivanova, E.A. and Meisser, N. (2007) Yakovenchukite-(Y), $K_3NaCaY_2(Si_{12}O_{30})(H_2O)_4$, a new mineral from the Khibiny massif, Kola Peninsula, Russia: A novel type of octahedral-tetrahedral open-framework structure. *American Mineralogist*, **92**, 1525–1530.

Kuebler, K.E., Wang, A. and Jolliff, B.L. (2011) Review of terrestrial laihunite and stilpnomelane analogs, identified as potential secondary alteration phases in MIL 03346. *Abstracts, 42nd Lunar and Planetary Science Conference*, p. 1022.

Krüger, H., Tropper, P., Haefeker, U., Tribus, M., Kahlenberg, V., Wikete, C., Fuchs, M. and Olieric, V. (2013) Innsbruckite, IMA 2013-038. CNMNC Newsletter No. 17, October 2013, page 2999; *Mineralogical Magazine*, **77**, 2997–3005.

Liebau, F. (1985) *Structural Chemistry of silicates – Structure, Bonding, and Classificatio*n. Springer-Verlag, Berlin.

McKeown, D.A., Bell, M.I. and Etz, E.S. (1999*a*) Raman spectra and vibrational analysis of the trioctahedral mica phlogopite. *American Mineralogist*, **84**, 970–976.

McKeown, D.A., Bell, M.I. and Etz, E.S. (1999*b*) Vibrational analysis of the dioctahedral mica: $2M_1$ muscovite. *American Mineralogist*, **84**, 1041–1048.

Moore, P.B. (1975) Laueite, pseudolaueite, stewartite and metavauxite: a study in combinatorial polymorphism. *Neues Jahrbuch für Mineralogie, Abhandlungen*, **123**, 148–159.

Peacor, D.R., Essene, E.J., Simmons, W.B., Jr. and Bigelow, W.C. (1974) Kellyite, a new Mn-Al member of the serpentine group from Bald Knob, North Carolina, and new data on grovesite. *American Mineralogist*, **59**, 1153–1156.

Petříček, V., Dušek, M. and Palatinus, L. (2006) *Jana2006. The Crystallographic Computing System*. Institute of Physics, Prague, Czech Republic.

Ralph, J. (2014) Mindat.org; http://www.mindat.org. Accessed May 2014.

Robinson, K., Gibbs, G.V. and Ribbe, P.H. (1971) Quadratic elongation: a quantitative measure of distortion in coordination polyhedra. *Science*, **172**, 567–570.

Rouse, R.C., Peacor, D.R., Dunn, P.J., Su, S.C., Chi, P.H. and Yeates, H. (1994) Samfowlerite, a new Ca Mn Zn beryllosilicate mineral from Franklin, New Jersey: its characterization and crystal structure. *The Canadian Mineralogist*, **32**, 43–53.

Spek, A.L. (2009) Structure validation in chemical crystallography. *Acta Crystallographica*, **D65**, 148–155.

Wahle, M.W., Bujnowski, T.J., Guggenheim, S. and Kogure, T. (2010) Guidottiite, the Mn-analogue of cronstedtite: a new serpentine-group mineral from South Africa. *Clays and Clay Minerals*, **58**, 364–376.

Wang, G., Yan, W., Chen, P., Wang, X., Qian, K., Su, T. and Yu, J. (2007) $Na_{2.4}CeSi_6O_{15}\cdot 2.6H_2O$: Hydrothermal synthesis, characterization and properties of a new luminescent microporous cerium silicate. *Microporous and Mesoporous Materials*, **105**, 58–64.

Wang, X., Liu L. and Jacobson, A.J. (2002) Open-framework and microporous vanadium silicates. *Journal of the American Chemical Society*, **124**, 7812–7820.

Yakovenchuk, V.N., Krivovichev, S.V., Pakhomovsky, Y.A., Ivanyuk, G.Y., Selivanova, E.A., Men'shikov, Y.P. and Britvin, S.N. (2007) Armbrusterite, $K_5Na_6Mn^{3+}Mn^{2+}_{14}[Si_9O_{22}]_4(OH)_{10}\cdot 4H_2O$, a new Mn hydrous heterophyllosilicate from the Khibiny alkaline massif, Kola Peninsula, Russia. *American Mineralogist*, **92**, 416–423.

Yamnova, N.A., Egorov-Tismenko, Y.K. and Khomyakov, A.P. (1996) Crystal structure of a new natural (Na,Mn,Ti)-phyllosilicate. *Crystallography Reports*, **41**, 239–244.